scientific data

OPEN

DATA DESCRIPTOR

A Frontal Ablation Dataset for 49 Tidewater Glaciers in Greenland

Dominik Fahrner[1,11]✉, Donald A. Slater[2], Aman KC[3], Claudia Cenedese[4], David A. Sutherland[1], Ellyn Enderlin[3], M. Femke de Jong[5], Kristian K. Kjeldsen[6], Michael Wood[7,8], Peter Nienow[2], Sophie Nowicki[9] & Till J. W. Wagner[10]

Frontal ablation at tidewater glaciers, which comprises iceberg calving and submarine and subaerial melting, is a key boundary condition for numerical ice sheet models but remains difficult to measure *in-situ*. Although previous studies have provided frontal ablation estimates over a range of spatiotemporal scales, most use ice discharge as an approximation, thereby neglecting the influence of terminus position change. Here, we present a dataset of frontal ablation estimates for 49 tidewater glaciers in Greenland that have reliable near-terminus bathymetry data. Near-terminus volume change over the period 1987–2020 is determined using previously published datasets of terminus positions (TermPicks) together with ice thicknesses estimated from ArcticDEM, AeroDEM, and Bedmachine v5 bed topography. Assuming a vertical terminus geometry and uniform ice density, we estimate frontal ablation as the residual between mass flux towards the terminus taken from a published dataset and mass change due to changes in terminus position. The frontal ablation dataset offers opportunities for developing new insights into ice dynamics, including helping to improve numerical model hindcasting and projections.

Background & Summary

Greenland's tidewater glaciers have been accelerating and retreating since the mid-1990's and contribute ~30–60% of the total annual mass loss from the Greenland Ice Sheet (GrIS) through frontal ablation[1–3]. A recent study estimated that the ice loss from calving front retreat alone has contributed ~1000 Gt to the total mass loss of the GrIS since 1985[4]. Frontal ablation, which comprises iceberg calving, submarine melting and subaerial melting at the glacier terminus[5], can be an important component of glacier mass balance and is susceptible to changes over a wide range of time scales (e.g., through changes in ice flow, ocean or air temperatures, or near terminus sea-ice or mélange conditions[6,7]). The mass flux of ice across a fixed gate (referred to as discharge) is often used to approximate frontal ablation, but this assumption does not take terminus position change into account[8].

Studies that do determine frontal ablation while also accounting for terminus position change have been conducted over varying spatio-temporal scales[4,9–14] and using a variety of data[15–17]. However, *in-situ* observational data, especially for the GrIS, are often lacking and satellite remote sensing data are temporally limited by image availability. Multi-decadal estimates of frontal ablation are therefore often confined to specific locations[10], limited time periods[15,17] or coarse temporal resolution[13]. Here we present a dataset of frontal ablation estimates that differs from previous work[13] in that it covers a large number of glaciers while resolving seasonal variability. Our dataset estimates frontal ablation as the residual between mass flux towards the terminus (estimated from ice discharge data) and mass change due to terminus position movement. This differs from a recent study[4] that considered only the mass change due to terminus position movement. In addition, the frontal ablation dataset we created here accounts for ice thickness change over time, which is typically assumed constant[4,13].

[1]University of Oregon, Department of Earth Sciences, Eugene, OR, USA. [2]University of Edinburgh, School of Geosciences, Edinburgh, UK. [3]Boise State University, Department of Geosciences, Boise, ID, USA. [4]Woods Hole Oceanographic Institution, Physical Oceanography Department, Falmouth, MA, USA. [5]Royal Netherlands Institute for Sea Research, Yerseke, the Netherlands. [6]Geological Survey of Denmark and Greenland, Department of Glaciology and Climate, København, Denmark. [7]Moss Landing Marine Laboratories, San José State University, Moss Landing, CA, USA. [8]Jet Propulsion Laboratory, California Institute of Technology, Pasadena, CA, USA. [9]University at Buffalo, Department of Geology, Buffalo, NY, USA. [10]University of Wisconsin-Madison, Department of Atmospheric and Oceanic Sciences, Madison, WI, USA. [11]Present address: Geological Survey of Denmark and Greenland, Department of Glaciology and Climate, København, Denmark. ✉e-mail: domfa@geus.dk

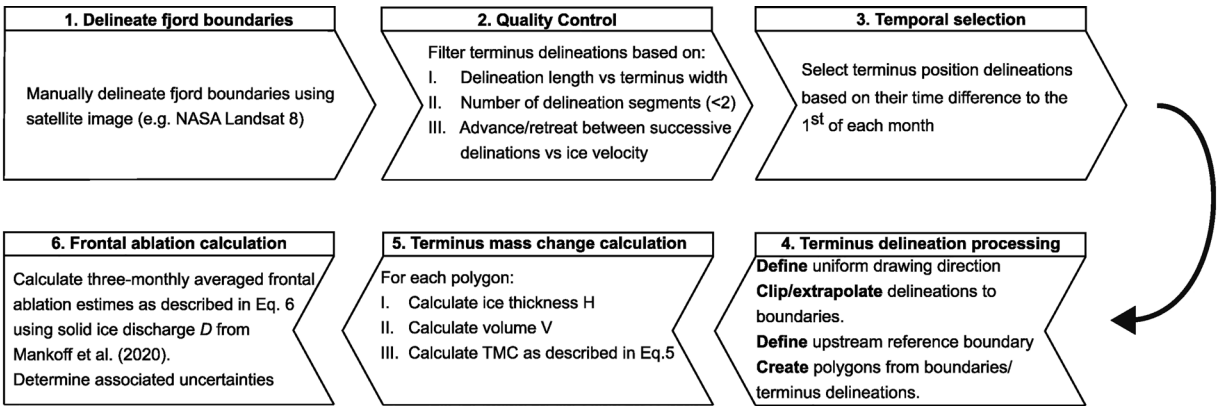

Fig. 1 Processing chain workflow. Schematic workflow for the calculation of frontal ablation estimates from observational data.

At all tidewater glaciers, there is a competition of processes that determine whether termini advance, retreat or remain stable. The ice velocity at the terminus advects the terminus forwards, while calving and melting of subaerial and submarine portions of the ice face move the terminus backwards (i.e., in the direction opposite to ice flow). This change in terminus position, L, is integrated over the frontal area of the terminus to give the following mass balance:

$$\int_A \frac{dL}{dt} dA = \int_A v dA - \int_A (c + m_s + m_a) dA \tag{1}$$

where v is ice velocity at the terminus, c is calving rate, m_s is submarine melt rate and m_a is subaerial melt rate. Each of these quantities may vary with depth or width along the calving front but in Eq. 1, we integrate over the terminus frontal area A. We define $\frac{dL}{dt}$ as positive for glacier advance and negative for glacier retreat. We define frontal ablation, F, as the sum of calving, submarine melting, and subaerial melting rates; that is all the processes that remove ice from the calving front, where:

$$F = \rho_i \int_A (c + m_s + m_a) dA, \tag{2}$$

and the ice density ρ_i is included so that F is a mass flux. Quantifying frontal ablation directly by estimating calving rate, submarine melt rate and subaerial melt rate is extremely challenging with large observational uncertainties. However, F can be estimated as the residual from Eq. 1, so that:

$$F = \rho_i \int_A v \, dA - \rho_i \int_A \frac{dL}{dt} dA, \tag{3}$$

which expresses frontal ablation in terms of ice velocity v and terminus position change $\frac{dL}{dt}$. If we assume that these are depth-invariant (i.e., assuming a vertical terminus face and plug flow for the ice velocity), then Eq. 3 can be rewritten as

$$F = \rho_i \int_W H v dW - \rho_i \int_W H \frac{dL}{dt} dW, \tag{4}$$

where H is ice thickness and W the width of the glacier. Each variable in Eq. 4 can be estimated from readily available remote sensing datasets. Hence, Eq. 4 provides a practical means of estimating frontal ablation. Note that the first term on the right-hand side of Eq. 4 is commonly referred to as the solid ice discharge D[18] so that frontal ablation differs from solid ice discharge D by the mass change relating to terminus position change (hereafter referred to as *Terminus Mass Change* or *TMC*). We neglect the variability in ice density (ρ_i)[13,19] and calculate *TMC* as the difference between two volumes V_1 and V_2 separated by a time $\Delta t = t_2 - t_1$:

$$\mathrm{TMC} = \rho_i \frac{V_2 - V_1}{t_2 - t_1}, \tag{5}$$

In this case we can approximate Eq. 4 as

$$F = D - TMC. \tag{6}$$

We process observational input data to ultimately determine frontal ablation[5] using Eq. 6 following the processing steps shown as a schematic in Fig. 1. We use the workflow as an outline for the remainder of the paper.

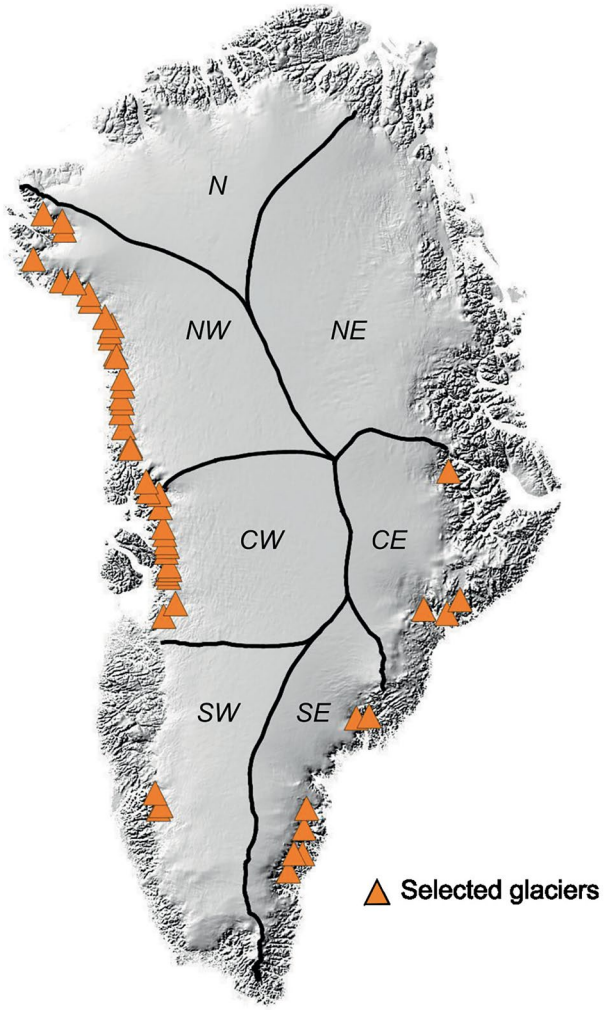

Fig. 2 Overview of Selected tidewater glaciers. Location of tidewater glaciers that have been selected for this study based on the reliability of bathymetry data. Basemap is taken from BedMachine v5[20,22]; Black lines show drainage basins after Mouginot and Rignot[2].

Methods

We select 49 of Greenland's more than 200 tidewater glaciers based on the uncertainty in their respective fjord bathymetry (Fig. 2; for a list of included glaciers, see Supplementary Table 1)[20–22]. We include glaciers only where bedrock topography data were derived from measurements, mass conservation or the GIMP DEM (as classified in the BedMachine v5 dataset), thereby excluding those glaciers where bedrock topography was derived synthetically or by interpolation, kriging, or gravity inversion[20,22] as these methods produce less reliable bathymetry and therefore larger uncertainties on ice thickness.

A brief overview of the input data which were used to calculate frontal ablation is given below, with the spatial resolution and temporal coverage of each input dataset as well as the associated uncertainties provided in Table 1.

- **NASA Landsat 8 satellite images** are used for the manual delineation of fjord boundaries. Data can be downloaded from https://earthexplorer.usgs.gov (requires account).
- **TermPicks terminus position data version 1**[23,24] are used to define the glacier terminus positions. The data can be found at https://doi.org/10.5281/zenodo.6954113.
- **ArcticDEM strips v 4.1**[25]**/AeroDEM**[26] are used for the calculation of surface elevation for each terminus position observation. While other Mosaic DEMs with a time stamp exist[27], almost no data are available for most glacier termini investigated in this study. ArcticDEM data can be found at https://doi.org/10.7910/DVN/OHHUKH. AeroDEM data can be found at https://doi.org/10.7289/v56q1v72.
- **Surface elevation change data**[28] derived from airborne and satellite altimetry are used where available to include annual surface elevation change. The data can be found at https://doi.org/10.22008/FK2/GQJJEA.
- **BedMachine v5 bed topography**[20,22] data are used to define the ice base for each terminus position observation. The data can be found at https://doi.org/10.5067/GMEVBWFLWA7X.

Parameter	Source	Spatial resolution	Temporal coverage	Uncertainty	Coordinate Reference System
Satellite imagery	NASA Landsat 8	15 m	single date	30 m horizontal	Location specific; reprojected to EPSG: 3413
Terminus position	TermPicks	15–30 m	1908–2020	30 m horizontal	EPSG: 3413
Surface elevation	ArcticDEM strips v4.1	2 m	2011–2018	0.1 m vertical	EPSG:3413
	AeroDEM	25 m	1978–1987	6 m vertical	Location specific; reprojected to EPSG:3413
Surface elevation change rate	Khan (2023)	1995–2011: 2 km 2012–2020: 2.5 km	1995–2020	Not provided	EPSG:4326; reprojected to EPSG: 3413
Bathymetry	Bedmachine v5	150 m	—	Variable; see Table S1	EPSG: 3413
Solid ice discharge	Mankoff *et al.* (2020)	N/A	1985-present	Variable[29]	EPSG:3413
Ice velocity (for filtering only)	MEaSUREs ITS_LIVE	240 m	1985–2019 (annual mean)	not needed for frontal ablation calculation	EPSG:3413

Table 1. Input data overview. Input parameters, data source, spatial resolution, temporal coverage, and associated uncertainties for previously published datasets used in this study.

- **Solid ice discharge data**[18,29] are required for calculation of frontal ablation estimates as described in Eq. 6. The data can be found at https://doi.org/10.22008/promice/data/ice_discharge/d/v02
- **Composite annual mean ice velocity data** from NASA's Making Earth System Data Records for Use in Research Environments (MEaSUREs) Inter-Mission Time Series of Land Ice Velocity and Elevation. The velocity data are generated using auto-RIFT[30] and provided by the NASA MEaSUREs ITS_LIVE project[31]. The data are used for filtering of terminus positions (see below) and can be found at https://doi.org/10.5067/IMR9D3PEI28U.
- **Centerlines and fjord boundaries** are provided for the investigated glaciers but must be manually drawn by the user if the processing chain is applied to other glaciers.

Fjord boundaries, temporal selection, and quality control. Before processing the glacier termini, we first define the fjord boundaries for each glacier (Fig. 1, step 1). These boundaries are created by manually delineating the fjord walls on either side of the glacier (hereafter referred to as fjord boundary 1 and 2) at a scale of 1:10,000 using pansharpened NASA Landsat 8 imagery at 15 m spatial resolution. The extent of the fjord boundaries starts at the mouth of the fjord where possible (otherwise past the most advanced terminus position) and ends upstream of the most retreated terminus position while allowing for enough space so that the (arbitrary) upstream boundary can intersect both fjord walls (e.g. Figure 5C). The coordinates of the boundaries are saved so that this step needs to be completed only once. It should be noted here that, since we keep the fjord boundaries fixed through time, any lateral thinning of the glacier is not considered. However, the associated uncertainty introduced is small compared to the other uncertainties (see below). Where the glacier terminus has extended into the ocean, the fjord boundaries are determined by using the endpoints of the terminus delineations as well as any natural bedrock features (e.g. islands).

The TermPicks delineations[23] of all investigated tidewater glacier termini are first visually examined to identify obvious outliers caused by e.g., inaccurate orthorectification of the satellite image, delineation of mélange or, in the case of Jakobshavn Isbræ, delineations of only one branch of the terminus. Subsequently, the monthly terminus observations are filtered to remove erroneous delineations and to ensure consistency in the dataset (Fig. 1, step 2). The filtering is conducted in sequential steps as follows:

1) We determine fjord width by calculating the distance between individual vertices of the previously created fjord boundaries, and terminus width by calculating the length of the individual delineation. Delineations which cover less than 95% of the terminus width, which is defined as the minimum distance between the two fjord walls, are excluded from further analysis (Fig. 3A). We also exclude terminus positions that are longer than the mean fjord width plus two standard deviations of the mean terminus length, as these are likely to include delineations of the fjord walls. This filtering step ensures that the delineations used for further analysis accurately represent the glacier terminus.
2) Terminus delineations are removed if they contain more than one line segment, which can occur, for example, if the terminus is split by a nunatak and the terminus has been delineated in two parts (Fig. 3A). While it would be possible to linearly interpolate between the line segments, this would skew the data and introduce additional uncertainties when combined with fully delineated termini.
3) We use NASA MEaSUREs ITS_LIVE ice velocity to filter out terminus traces that indicate the front has advanced faster than the ice velocity. The annual composite velocity images are automatically downloaded[32] when first running the code. Ice flow velocities are successively extracted along a centerline, which has been drawn manually for each glacier (available in the processing chain repository). The centerline method is chosen to ensure that velocities are representative of the terminus region and are not skewed by slower flowing parts of the glacier (e.g., lateral drag at the margins). The flow velocities are then averaged for the decade preceding the last available velocity observation to create a decadal mean value velocity. The use of a decadal mean ensures a high-quality velocity product which is used in filtering - shorter time periods can occasionally suffer from missing data. Terminus advance is determined using the normal n to the line connecting the intersection points (c_1 and c_2) of the centerline with successive delineations (t_1 and t_2; Fig. 3B). If the intersection point of the second delineation is located down-fjord of the normal, the glacier

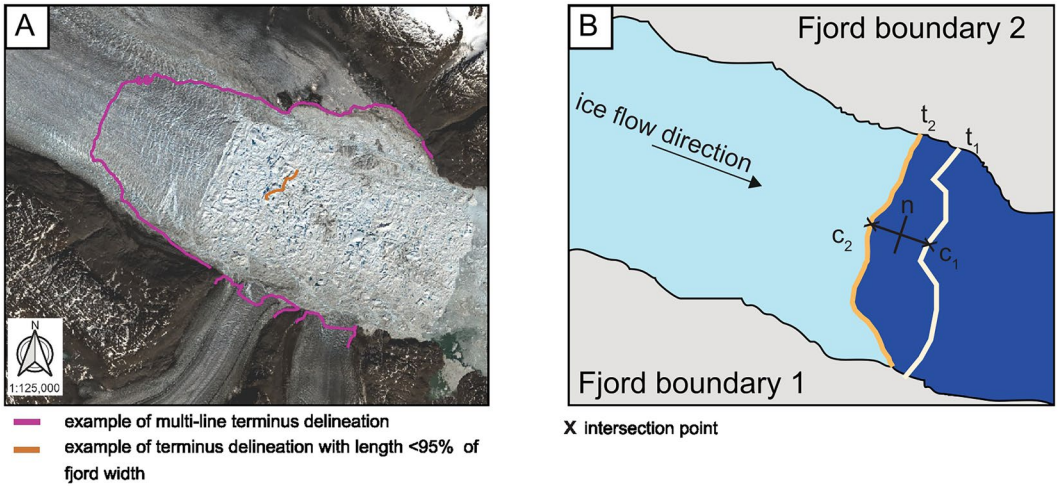

Fig. 3 Terminus delineation filtering. (**A**) Examples of terminus delineations with more than one line segment (pink) and with a length shorter than 95% of the fjord width (orange), which are excluded from the dataset. (**B**) Schematic showing how advance and retreat are determined. The normal (n) to the line connecting the intersection points (c_1 and c_2) of successive terminus delineations (t_1 and t_2) is used to determine advance and retreat of the glacier. In the sketch shown here, c_2 is up-fjord of the normal n, therefore the glacier has retreated. This classification of advance/retreat is solely used for filtering purposes.

movement is classified as advance. Terminus advance or retreat is quantified by calculating the distance between intersection points. To ensure that the delineations represent realistic changes in terminus positions, we then use the decadal mean ice velocity to infer how much the glacier could have advanced during each terminus observation timestep. If the terminus advance, as determined from the terminus delineations, is greater than twice the predicted flow velocity, the terminus delineation is considered erroneous and is excluded from the dataset. We deliberately use a high threshold of twice the mean decadal velocity so that rapidly advancing glaciers are not excluded from the dataset.

Note that this notion of terminus advance/retreat is used only in the terminus position filtering. The impact of terminus advance/retreat on frontal ablation is described in the 'Terminus delineation processing' section below.

During this phase we further exclude the originally selected glaciers Kjer and Nordenskiöld from the analysis as their fjord walls are extremely difficult to delineate, as well as Zachariae Isstrøm and Qeqertaarsuusarsuup Sermia due to their floating ice shelves, resulting in the final 49 selected systems. The manual delineation of ice shelves is challenging due to their complex structure and the difficulty of distinguishing between terminus and mélange. Overall, after quality control and sub-setting in time to one observation per month, the dataset contains 55.3% of all terminus delineations (10262 of 18556) for the selected 49 glaciers. We then subsampled the TermPicks dataset[23] by selecting terminus traces separated by approximately 1 month. We found that using terminus positions spaced at closer than 1 month gave unreliable frontal ablation estimates (the uncertainty increases as the time interval decreases – see discussion of uncertainties below). We also found that delineations that are only several days apart and created by different authors can differ significantly and thereby introduce large uncertainties[cf.24]. Since terminus delineations are typically not separated by exactly one month, we select the first available trace within each monthly period (Fig. 1, step 3). At a later stage, a further sub-selection of terminus traces to three-monthly or annual resolution can be made, which defines the temporal resolution of the frontal ablation estimate. Finally, we restricted the terminus positions used to those observed within the period of ice discharge estimates (1986-present)[29].

We note here that there are data gaps within the monthly time series of glacier specific terminus positions. An overview of the number of terminus positions pre- and post-filtering can be found in Supplementary Figure 1. The filtered delineations are saved in ESRI shapefile format for manual quality control.

Terminus delineation processing. Even after filtering, tidewater glacier terminus positions in the TermPicks dataset vary widely in their length and differ in their starting/end points. For example, traces for an individual glacier could be drawn in opposing directions (e.g., from North to South as well as South to North), which will be referred to as drawing direction hereafter, depending on the author. The drawing direction is important to locate the individual terminus delineations in space with respect to the fjord boundaries. We therefore standardized the drawing direction based on the distance between the terminus delineation endpoint and the fjord boundaries. If the end point of the terminus delineation is located closer to the fjord boundary 1 than fjord boundary 2, the terminus start and end points are switched.

To accurately compute terminus area change using the filtered time series of terminus delineations, the length of each terminus position must be set to be consistent with the previously defined fjord boundaries. We therefore convert the fjord boundary polylines into polygons. If the start/end point lies within the respective boundary polygon, the terminus delineation is clipped, and the new start/endpoint is defined as the intersection

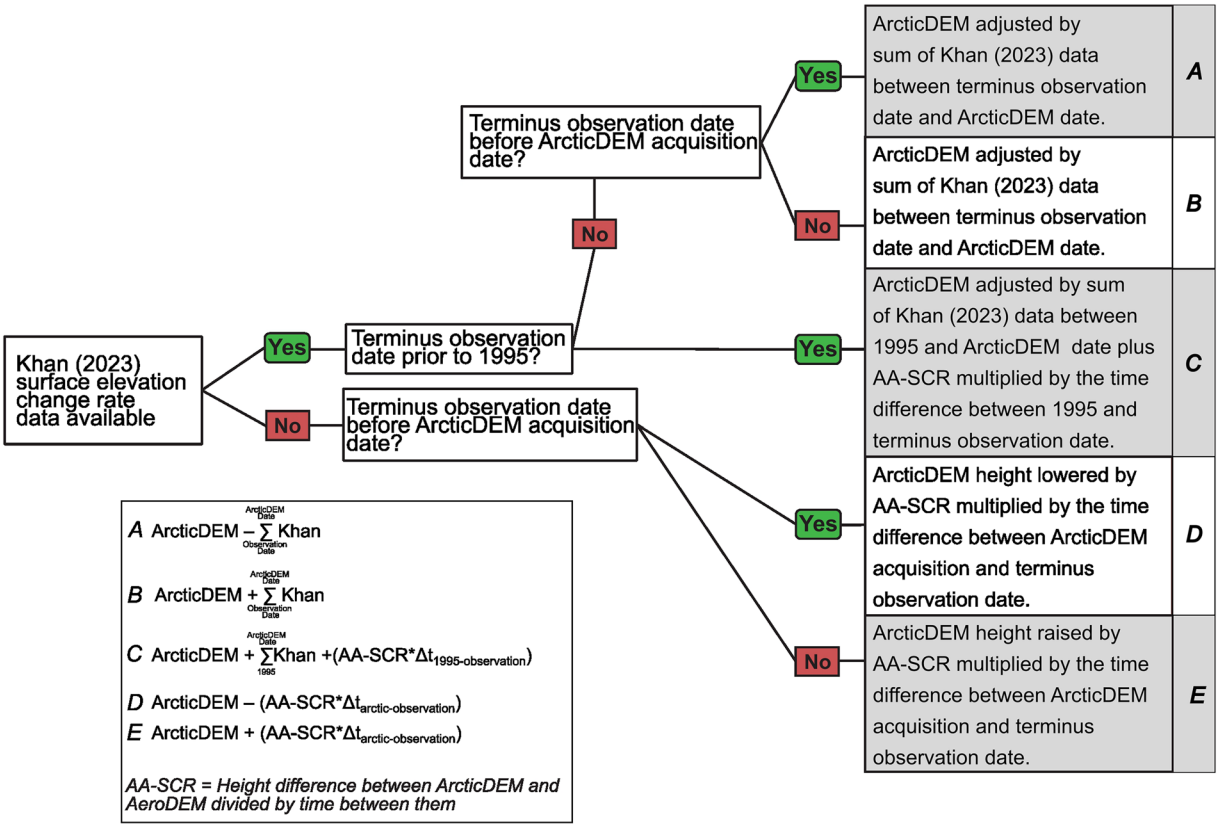

Fig. 4 Workflow for ice thickness calculation. Workflow schematic showing how surface elevation for a given terminus observation is determined based on the availability of surface elevation change rate data from Khan (2023). If no data is available or the terminus observation is outside of the temporal range of Khan (2023), we applied a linear surface elevation change rate, which is determined by first differencing the Arctic– and AeroDEM and dividing by the time difference between their time stamps to obtain annual surface elevation change (referred to as ArcticDEM-AeroDEM surface change rate or AA-SCR).

point between terminus delineation and fjord boundary polygon. If the point lies outside of the fjord boundary polygon, the terminus delineation is extrapolated to the nearest point on the boundary polygon. We compare the length of the extrapolation to the length of the manually delineated terminus trace to ensure that the majority of the terminus is captured by the latter. The observation is excluded if the length of the extrapolation exceeds the length of the delineated terminus. We do not account for the extrapolation in the overall uncertainties as we are unable to compare the extrapolation to data to determine the error.

Subsequently, an upstream reference boundary needs to be defined so that the area change resulting from terminus position change can be computed (Eq. 5). This upstream boundary is defined manually by drawing an arbitrary line upstream of the most retreated position of the glacier that intersects both manually delineated fjord boundaries on top of a pansharpened true color NASA Landsat 8 image. The reference boundary is fixed and remains the same for all terminus positions at a given glacier over time. 2-D polygons can then be created for each terminus observation by combining the reference boundary, fjord boundaries, and terminus delineation.

Terminus mass change calculation. The 2-D polygons created above provide the basis for the calculation of area, volume and mass. To obtain polygon volume, we estimate ice surface elevation at the time of each individual terminus observation by combining three datasets (Table 1):

i) 2 m DEM strips from ArcticDEM acquired within the last decade[25];
ii) an AeroDEM from 1981 or 1985[26];
iii) Khan (2023) surface elevation change rates from altimetry[28].

The ArcticDEM and AeroDEM are registered to the WGS 84 ellipsoid and were resampled to a common grid, taken to be the 150 m resolution grid of the BedMachine v5 bed topography data. The Khan (2023) surface elevation change rate data is provided as point data with two different resolutions of 2 km for the period 1995–2011 and 2.5 km for the period 2012–2020. The lower resolution data is resampled to a 2 km grid using linear interpolation so that we obtain a combined dataset for the period 1995–2020 with a 2 km resolution. Using the previously created polygons, we extract surface elevation change rates for the points that lie within the polygon. We take the baseline surface elevation to be the most recent ArcticDEM strip, and then adjust the elevation from this as follows (schematically illustrated in Fig. 4):

a) If data from Khan (2023) are unavailable, we apply a linear surface elevation change rate. This rate (referred to as ArcticDEM-AeroDEM Surface Change Rate or AA-SCR) is determined by first differencing the ArcticDEM and AeroDEM and dividing by the time difference between their time stamps to obtain annual surface elevation change. For each terminus observations, the adjustment of elevation from the ArcticDEM is then obtained by multiplying the AA-SCR by the time interval between the terminus position observation and the ArcticDEM acquisition date. Depending on whether the date of the terminus position observation is before or after the acquisition date of the baseline DEM, the surface elevation is raised or lowered, respectively.
b) If surface elevation change rates are available from Khan (2023) – which is not the case for every glacier in our dataset due to incomplete spatial coverage in their dataset –the annual values are applied to the baseline DEM until the terminus observation date is reached. Prior to 1995, when Khan data are not available, we apply the AA-SCR multiplied by the time difference between terminus observation date and 1995 to the surface elevation that has been determined for 1995 using the Khan (2023) data.

Thus, we obtain a surface elevation estimate at the time of each terminus delineation, enabling the calculation of ice thickness H as the difference between the surface elevation and the underlying bedrock topography extracted along the centerline from Bedmachine v5[20,22].

With the calculated ice thickness, we create 3-D polygons and determine the ice mass for each terminus observation using an ice density of 917 kg/m^3. We note that significant crevassing near tidewater glacier termini means that the effective density of part of the polygon will be lower than that of pure ice. However, the impact is likely small as a previous study found that for a heavily crevassed tidewater glacier the column mean density near the front is reduced to 908 kg/m^3 [33], which corresponds to a <1% correction to the mass estimates above.

Frontal ablation calculation. Strictly, we require the solid ice discharge at the glacier terminus to calculate frontal ablation, yet the flux gates used to derive solid ice discharge are located approximately 5 km upstream of the terminus[18]. While acknowledging that there could be a time lag or a small difference (~5%[18]) between discharge at the flux gate and the terminus, we note that fast flowing tidewater glaciers have strong longitudinal stress coupling[34], thus we assume that the discharge at the upstream flux gates is representative of the flux at the terminus.

The ice discharge (D) data are temporally matched to the previously determined timeseries of terminus mass change (TMC), and both timeseries are subsequently linearly interpolated to the first of the month. Mass change over the month (in Gt/d) is then calculated as the difference in the mass divided by the number of days in the month. Using these standardized timeseries, we can calculate frontal ablation F directly from Eq. 6. The processing chain provides the options to estimate monthly, three-monthly or annual frontal ablation. Note that with the applied interpolation and averaging, the results should be interpreted as the mean value over the time in question. We recommend use of the three-monthly or annual estimates because the monthly estimates are more susceptible to errors in the terminus delineation induced, for example, by pixel size of the satellite image or individual delineation error.

Figure 5A shows an example of the three-monthly mean frontal ablation estimates in the dataset for Helheim Glacier, Southeast Greenland. Corresponding terminus position change relative to the most recent observation and the terminus delineations used in the calculation are shown in Fig. 5B, C. Frontal ablation shows a high degree of seasonal variability (Fig. 5A), which is imparted by seasonal advance and retreat of the terminus position (Fig. 5C). From 1996–2001, however, there is muted seasonal variability in frontal ablation as the terminus position and ice velocity are nearly constant in time. From 2001–2006, frontal ablation exceeded the ice discharge by an average of 14%, leading to the dramatic retreat of Helheim during this period[35,36]. It is apparent from Fig. 5A that frontal ablation estimates that take terminus change into account show a higher seasonal variability than those derived from ice discharge alone[18].

Figure 6A provides an overview of the annual mean frontal ablation (expressed as marker size in Fig. 6A) as well as the annual mean proportion of TMC (yellow) and solid ice discharge (green) for each tidewater glacier. The aggregate line plot in Fig. 6B further highlights the higher seasonal variability of frontal ablation when including terminus position observations compared to those derived from solid ice discharge. The three-monthly mean frontal ablation estimates for all glaciers can be found in Supplementary Table S1.

Uncertainties. The input data products described above contain glacier- and time-dependent uncertainties (denoted with δ), that must be accounted for in the frontal ablation estimates produced here. To quantify uncertainty in frontal ablation estimates for each individual tidewater glacier investigated in this study, we use standard methods to propagate the uncertainties of the input data products through the processing chain.

Frontal ablation is calculated as the difference between solid ice discharge and terminus mass change at the terminus (Eq. 6)[5]. Therefore, if the solid ice discharge uncertainty is δD[29] and the TMC uncertainty is δTMC, then the uncertainty in frontal ablation δF is:

$$\delta \mathrm{F} = \sqrt{(\delta \mathrm{D})^2 + (\delta \mathrm{TMC})^2}\,. \tag{7}$$

As outlined in Eq. 5, we could determine δTMC by estimating the uncertainty on V_1 and V_2 and combining those; however, this would not take into account the fact that the uncertainty on the fjord width and bedrock topography are systematic (i.e., the same uncertainty exists on both volumes; see Supplementary Table S1 for mean bedrock topography uncertainty, which is extracted along the centerline thereby excluding shallow areas near the lateral fjord boundaries). Therefore, we schematically take the difference between the volumes to be a

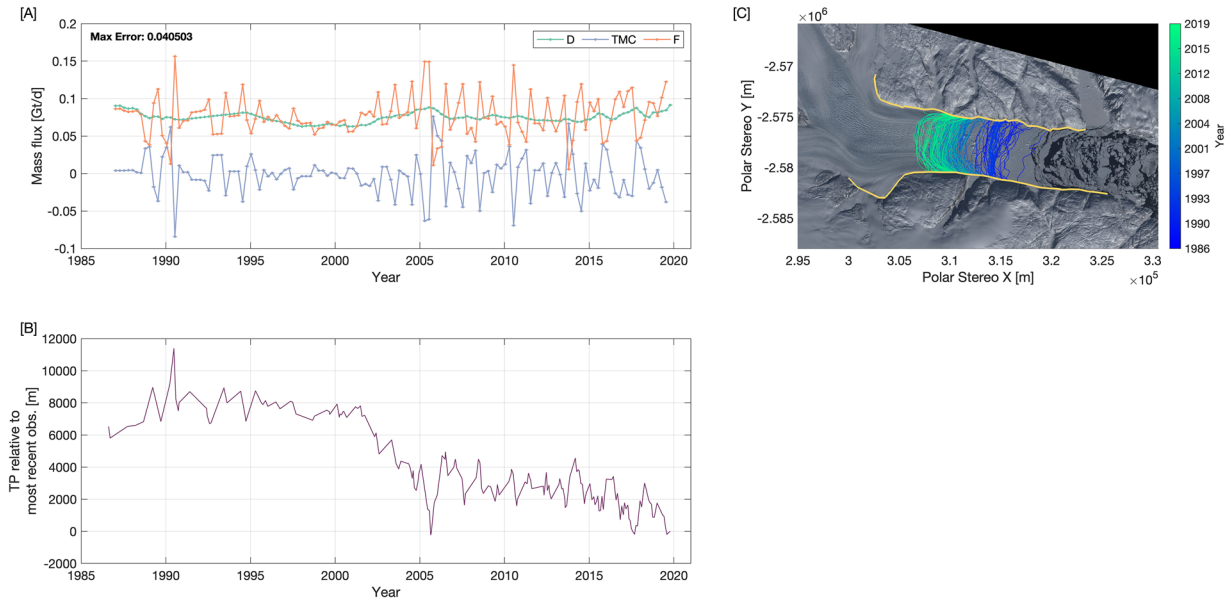

Fig. 5 Example of output data. (**A**) Example of frontal ablation estimates (orange), terminus mass change (blue) and ice discharge (green) for Helheim Glacier, SE Greenland. (**B**) Terminus position (TP) change relative to the most recent observation. (**C**) Processed terminus delineations used for the calculation of frontal ablation estimates shown in (**A**) colour-coded by date. Basemap is a pan-sharpened Landsat 8 image with yellow lines showing the manually delineated fjord boundaries.

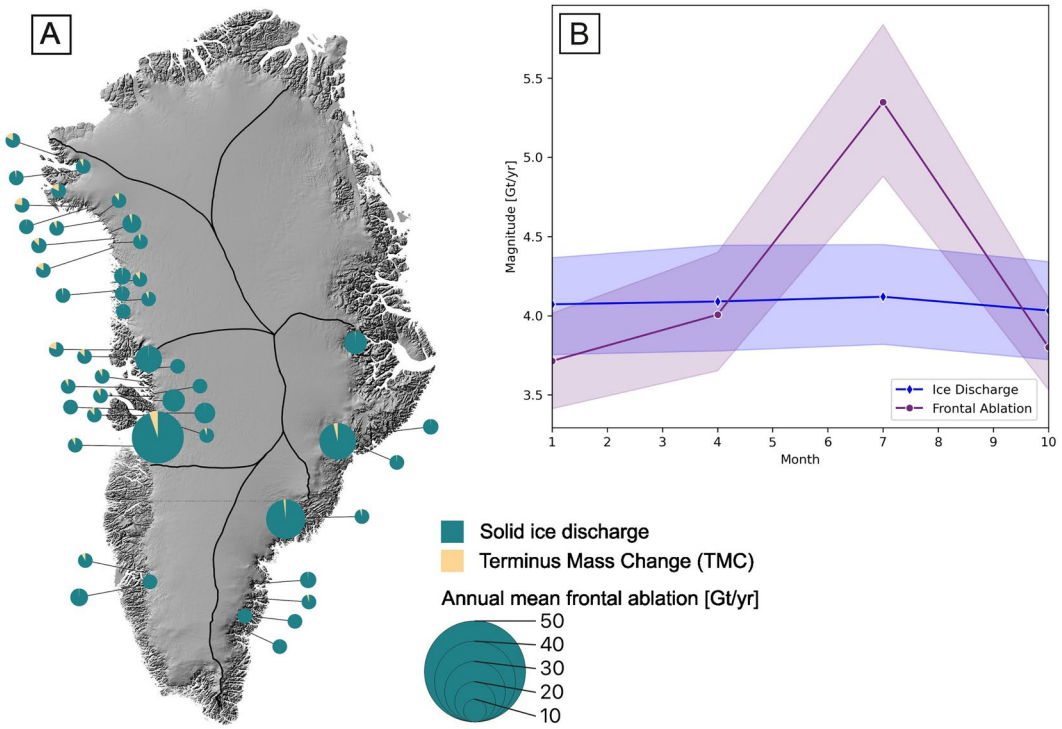

Fig. 6 Annual mean ice discharge and frontal ablation. (**A**) Annual mean solid ice discharge (green) vs. annual mean terminus mass change (TMC) estimates (yellow) for all glaciers investigated in this study. Circle size indicates annual mean frontal ablation. Basemap taken from BedMachine v5[20,22]; lines show drainage basins after Mouginot and Rignot[2]. (**B**) Aggregated line plot showing three-month average frontal ablation estimates (purple) vs solid ice discharge (blue) with respective 95% confidence intervals computed over the study period 1988–2018.

cuboid of width W, thickness H and length L (i.e., if the glacier has retreated between t_1 and t_2, then W is the fjord width, H is the ice thickness and L is the retreat length along the centerline) and combine the uncertainties on this differenced volume. We can then estimate the uncertainty on $V_2 - V_1$ as

$$\delta V = \sqrt{W^2H^2\delta L^2 + W^2L^2\delta H^2 + L^2H^2\delta W^2}, \tag{8}$$

with

$$\delta H = \sqrt{(\delta \text{ArcticDEM})^2 + (\delta \text{AeroDEM})^2 + (\delta \text{Bedrock topography})^2}. \tag{9}$$

We currently do not include uncertainties of the surface elevation change rates from Khan (2023) as no continuous errors for the complete timeseries are provided with the dataset.

The delineation uncertainties δL and δW are based on the satellite that was used to delineate the terminus position and fjord walls. While previous studies suggest relatively small delineation uncertainties, these estimates are for a single operator and only for Landsat 7/8 and Sentinel 1[37,38]. To account for multiple operators and varying satellites, we choose to keep the delineation uncertainty constant at 30 meters, which is twice the pixel resolution of the most recent satellites (e.g. Landsat 7, 8). Combining Eqs. 5 and 8, we can then determine the uncertainty on terminus mass change for each time-averaged step as:

$$\delta \text{TMC} = \frac{\rho_i}{t_2 - t_1}\delta V \tag{10}$$

where $t_2 - t_1$ is the time resolution of the frontal ablation dataset (31 days, 90 days, 365 days), with 90 days used here in our results. Equation 10 gives uncertainties that change in time, which are included in the dataset, but as a conservative approach, we report the maximum over the analysis period as a single value in our results (see below for details).

Data Records

The resulting data product contains frontal ablation estimates for 49 selected tidewater glaciers in Greenland from 1987–2020 at three-monthly resolution. Version 9 of the product is available as a merged file for all 49 glaciers as point geometry in NetCDF (FrontalAblationEstimates.nc), Shapefile (FrontalAblationEstimates.shp), and GeoPackage (FrontalAblationEstimates.gpkg) format in the following Zenodo repository: https://doi.org/10.5281/zenodo.10076252[39]. The data for all individual glaciers is projected onto the timeframe 15/01/1987–15/10/2020 for easy comparison and data gaps are filled with *Not A Number* (NaN) values. The files are stored in the folder FrontalAblationEstimates.zip. The following variables are contained in the NetCDF:

- **Time** – Midpoint of time intervals on which output data is defined [days since 01/01/1950]
- **Name** – Name of each glacier investigated in this study [unitless]
- **Lat** – Latitude (EPSG:4326) [degrees]
- **Lon** – Longitude (EPSG:4326) [degrees]
- **PolarX** – Polar Stereographic X Coordinate (EPSG:3413) [m]
- **PolarY** – Polar Stereographic Y Coordinate (EPSG:3413) [m]
- **F** – Three-month-average frontal ablation estimates during time intervals [Gt/d]
- **F_Max_U** – Maximum uncertainty over total time period [Gt/d]
- **F_U** – three-month-average frontal ablation uncertainty for time intervals [Gt/d]
- **D** – Three-month-average solid ice discharge during time intervals [Gt/d]
- **D_U** – Three-month-average solid ice discharge uncertainty for time interval [Gt/d]
- **TMC** – Terminus mass change (dM/dt) during time intervals [Gt/d]
- **TMC _U** – Three-month-average terminus mass change uncertainty during time intervals [Gt/d]
- **L** – Interpolated terminus change over time (L) [km]
- **Delta_L_W** – Delineation and fjord width uncertainty (δL, δW; constant) [km]
- **H** – Mean ice thickness within the polygon; maximum over the observation period (H) [km]
- **Delta_H** – Ice thickness uncertainty with constant ArcticDEM/AeroDEM uncertainties of 0.1 m and 6 m, respectively (δH) [km]
- **Rho** – Ice density (ρ_i; constant) [kg/km^3]
- **W** – Mean fjord width (W) [km]
- **Bedrock_U** – Mean uncertainty in bedrock topography along the centerline [km]
- **TI** – Time interval over which data are averaged ($t_2 - t_1$; 90 days for the results presented here) [d]

The shapefile and geopackage files contain the same the same variables as the NetCDF, however the variable Time is formatted differently for ease of use, and the variables Polar X and Polar Y are contained in the field geometry as outlined below:

- **Time** – Midpoint of time intervals on which output data is defined [yyyy-mm-dd]
- **Geometry** – Point geometry containing X and Y coordinates in Polar Stereographic Coordinate Reference System (EPSG:3413) [m]

Technical Validation

We compare our results against recently published, decadal mean frontal ablation estimates for the periods 2000–2010 and 2010–2020[13], as well as monthly catchment mass change estimates[4].

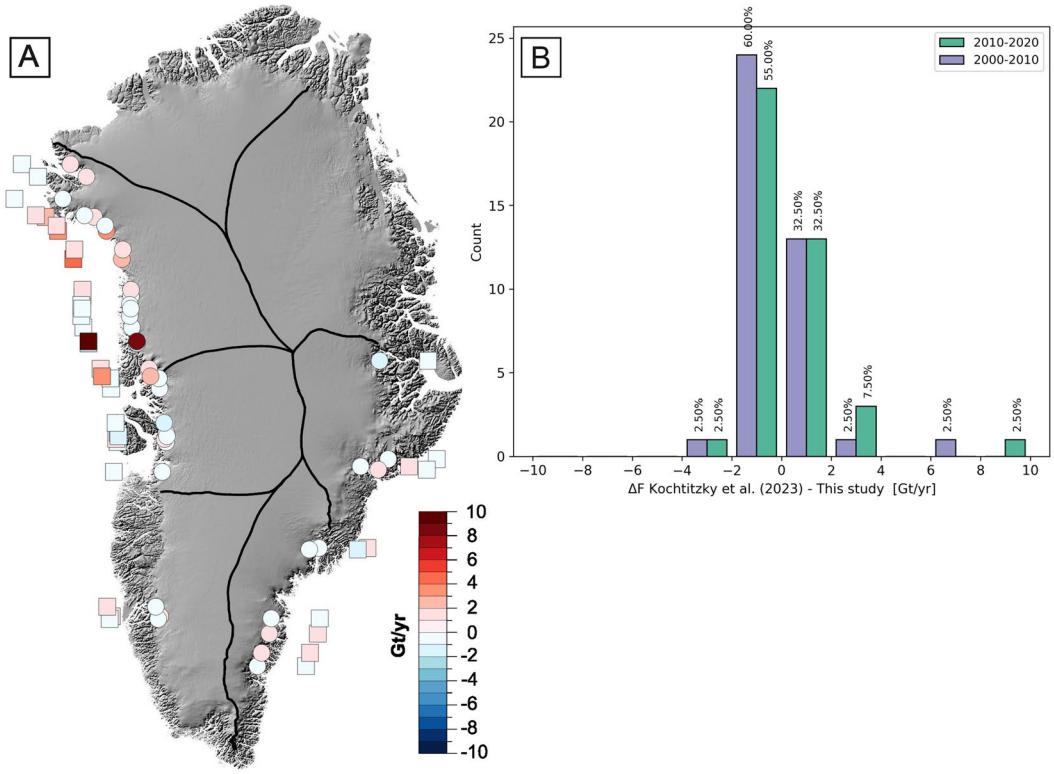

Fig. 7 Comparison of decadal frontal ablation estimates. (**A**) Map showing the difference between frontal ablation estimates from Kochtitzky *et al.*[13] and this study for each glacier for 2000–2010 (circle) and 2010–2020 (square). Basemap taken from BedMachine v5[20,22]; Black lines show drainage basins after Mouginot and Rignot[2]. (**B**) Histogram showing the difference between decadal mean frontal ablation estimates (ΔF) of Kochtitzky *et al.*[13] and the results presented in this study for 2000–2010 (purple) and 2010–2020 (green); percentage indicates the relative number of glaciers in each bin.

For the comparison of decadal values[13], we calculate decadal mean values for glaciers investigated in both studies from our dataset. We exclude Sermeq Kujalleq (Jakobshavn Isbræ) from the comparison as we do not account for floating ice in our calculation and therefore only provide data for this glacier after the break-up of the ice tongue in 2003[40]. The data for Sermeq Kujalleq (Jakobshavn Isbræ) is however provided in Table S2 for completeness. The results show that 60% (24 out of 40 glaciers) of our estimates are within 0.2 Gt/yr, and over 80% (33 out of 40 glaciers) are within ±1 Gt/yr of the uncertainty boundaries of Kochtitzky *et al.*[13] for both decadal periods (Fig. 7; Supplementary Table 2). For tidewater glaciers investigated in both studies, we estimate total decadal frontal ablation to be 164.67 ± 12.23 Gt/yr for the period 2000–2010, which agrees within uncertainty with the totals from the same glaciers in Kochtitzky *et al.* (169.83 ± 8.1 Gt/yr), and 162.78 ± 12.14 Gt/yr for the period 2010–2020 (175.95 ± 5.97 Gt/yr; 2023; Supplementary Table 2).

It should also be noted that our study uses a different solid ice discharge product compared to Kochtitzky *et al.*[13]. The flux gates used by Kochtitzky *et al.*[13] are positioned closer to the terminus and subaerial melting below the flux gate is excluded from their ice discharge, both of which can significantly influence the final frontal ablation estimates. For example, at Sermeq Kujalleq (Store Glacier), one of the glaciers with the largest difference between the two studies, the 2000–2010 mean ice discharge used in this study is 9.1 Gt/yr[29] compared to 7.9 Gt/yr in theirs[13].

In comparing our results to Kochtitzky *et al.*[13], we can remove the influence of the different ice discharge products by focusing only on what we have termed terminus mass change, TMC (called "absolute net Volume change" in the decadal data product[13]; Fig. 8). For this comparison, we calculate the annual mean TMC for each decade and each glacier. While our TMC estimates are largely not within the uncertainty boundaries[13], the comparison shows that the majority (>65%) of our results are within ±0.1 Gt/yr for both time periods (Fig. 8B). This highlights that the choice of ice discharge product for the calculation of TMC estimates can significantly influence the results.

We further compare our dataset to recently published monthly estimates of catchment mass[4]. To allow a direct comparison of these data to the dataset presented here, we apply the same three-monthly averaging to the catchment mass estimates and calculate mass change by differencing successive values. The results show that our terminus mass change estimates are in good agreement with those of Greene *et al.*[4], differing on average by ±1.5 Gt/yr (Fig. 9A). This is further apparent when comparing values for all glaciers individually (Fig. 9B,C), which corroborates that the majority (>68%) of our terminus mass change estimates are within ±0.5 Gt/yr of

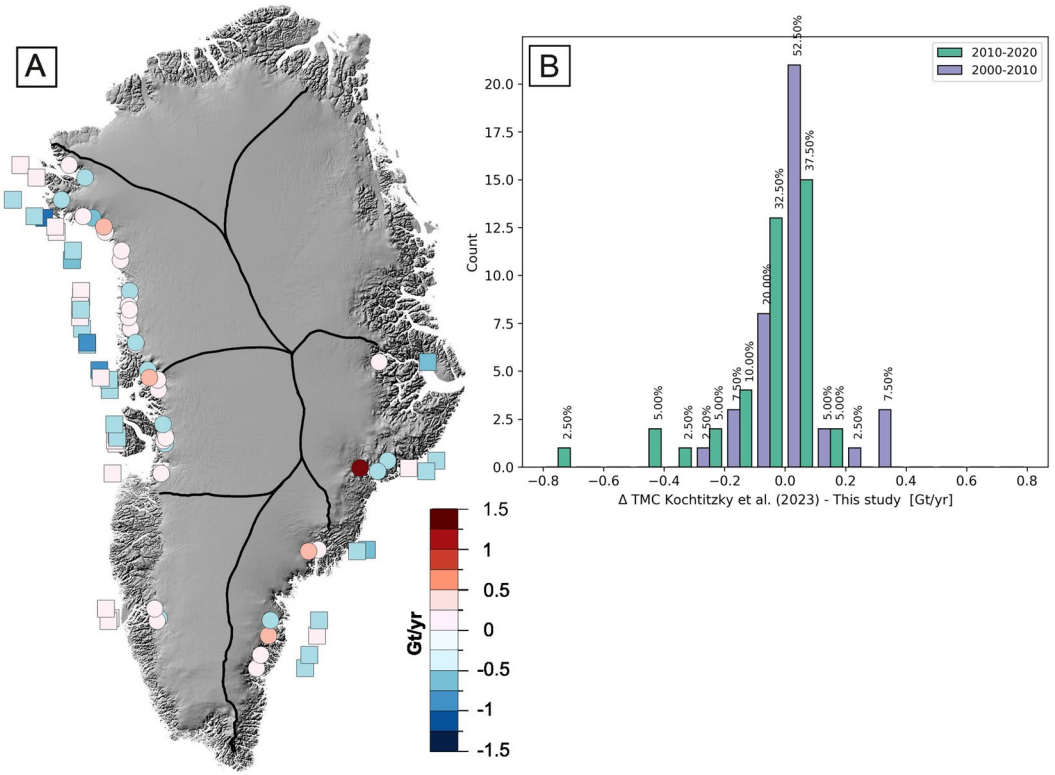

Fig. 8 Comparison of decadal terminus mass change estimates. (**A**) Map showing the difference between terminus mass change (TMC) estimates from Kochtitzky *et al.*[13] and this study for each glacier for 2000–2010 (circle) and 2010–2020 (square). Basemap taken from BedMachine v5[20,22]; Black lines show drainage basins after Mouginot and Rignot[2]. (**B**) Histogram showing the difference between decadal mean TMC estimates of Kochtitzky *et al.*[13] and the results presented in this study for 2000–2010 (purple) and 2010–2020 (green); percentage indicates the relative number of glaciers. Note: The histogram is zoomed in to highlight the range for the majority of values. The ΔTMC for Kangerlussaq Glacier is 1.15 Gt/yr and 0.011 Gt/yr for the periods 2000–2010 and 2010–2020 respectively.

the estimates of Greene *et al.*[4]. An overview of three-monthly averaged mass change differences between Greene *et al.*[4] and the results presented here for each glacier and timestep can be found in Supplementary Figure 2.

We use terminus position data from a multi-operator delineation dataset[23], so that delineations require preprocessing and filtering as well as temporal selection to exclude erroneous delineation. In comparison, Kochtitzky *et al.*[13] use a single-operator delineation dataset[13], and Greene *et al.*[4] use an ice flow model to validate compiled multi-operator delineations[4]. The differences in the input terminus position datasets and the subsequent processing may explain some of the apparent variations in frontal ablation estimates between the studies, especially for glaciers where the terminus geometry is complex. For Kangerlussuaq Glacier, for example, we find a significantly higher TMC for the period 2000–2010 compared to Kochtitzky *et al.*[13]. We attribute this to differences in ice thickness between the different dataset as Kochtitzky *et al.*[13] use a single value for each decade whereas we calculate ice thickness for each terminus observation. Another contributing factor to observed differences could be the definition of the fjord boundaries, as we exclude the shallow, slow flowing part at the northern margin based on the delineated terminus positions.

However, despite the different approaches between the previously published studies and the one presented here, there is general good agreement between the frontal ablation estimates.

The dataset presented here provides three-monthly frontal ablation estimates for 49 tidewater glaciers based on ice discharge and terminus position changes for each glacier. The dataset offers opportunities for the community to explore the drivers of mass loss at a large suite of tidewater glaciers around Greenland and provides the basis to improve current parameterizations of climate forcing of tidewater glacier mass loss, in both model hindcasting and projections.

The results highlight that frontal ablation can differ significantly from solid ice discharge. On a seasonal basis, frontal ablation can exceed ice discharge by more than 50% at some glaciers during the summer retreat phase, but conversely ice discharge can exceed frontal ablation by a similar magnitude during winter advance (Figs. 5, 6). Summed over all 49 glaciers, mean 1988–2018 frontal ablation (time period where data is available for all glaciers) of 227.54 Gt/yr (without Sermeq Kujalleq (Jakobshavn Isbræ): 179.23 Gt/yr) exceeds the mean ice discharge of 219.5 Gt/yr (173.76 Gt/yr). We find that total ice mass loss is underestimated by 3.6% (3.2%) if mass loss contributions from glacier retreat are ignored, supporting the findings of a previous study[4]. Overall, the results presented here are in good agreement with previously published datasets[4,13], when considering the sum of frontal

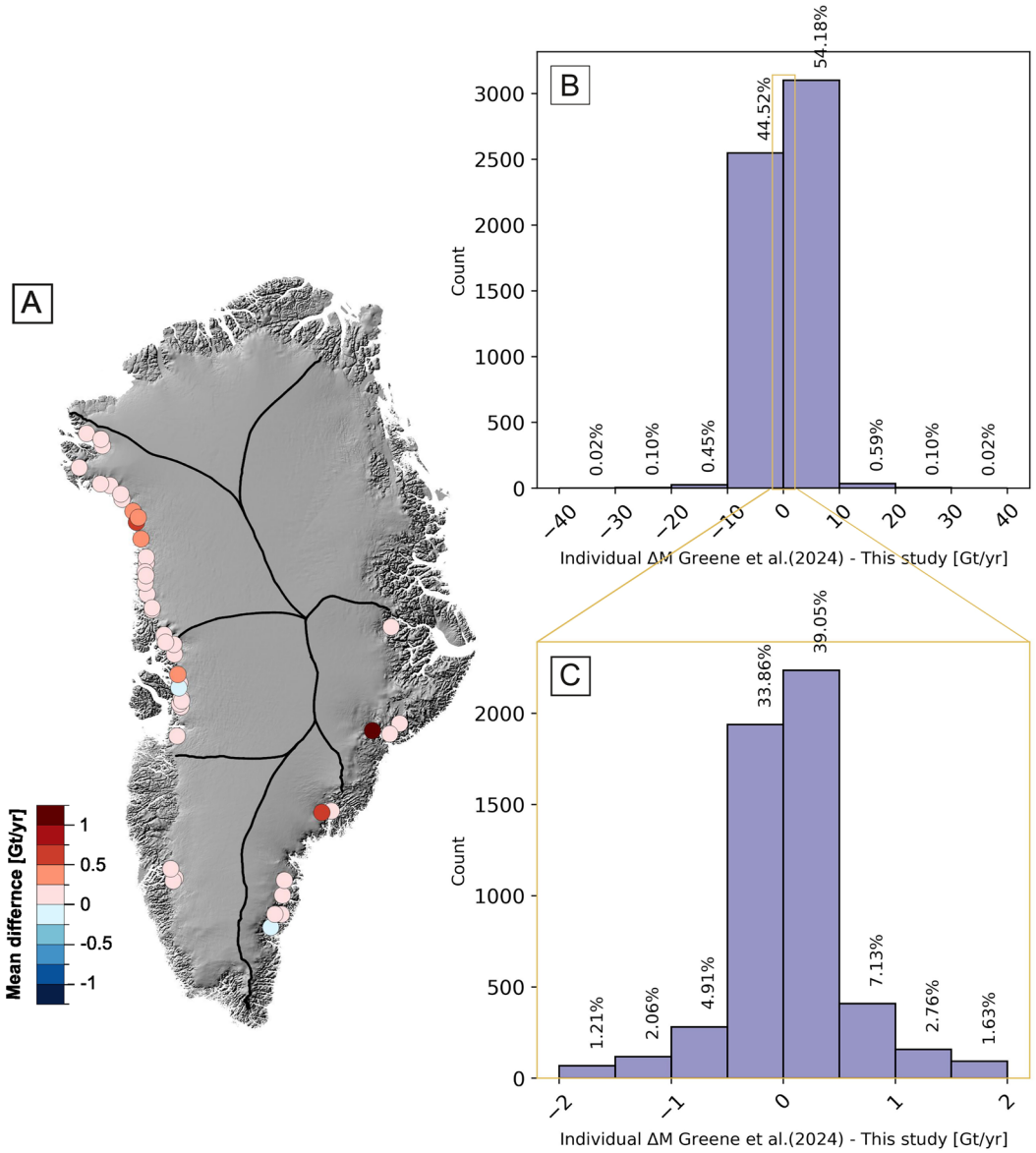

Fig. 9 Comparison of catchment mass change and terminus mass change. (**A**) Map showing the mean difference between three-monthly averaged catchment mass change[4] and three-monthly averaged terminus mass change from this study for each glacier. Basemap taken from BedMachine v5[20,22];Black lines show drainage basins after Mouginot and Rignot[2]. (**B**) Histogram showing the difference between individual three-monthly averaged catchment mass change estimates (ΔM) and three-monthly averaged terminus mass change (TMC) estimates from this study with percentage indicating the relative number of glaciers in each bin. (**C**) Zoomed in histogram of (**B**) to highlight that the majority of values fall between −0.5 and 0.5 [Gt/yr].

ablation across all our 49 study glaciers, although notable differences exist for a few individual glaciers, likely due to the differing methodologies applied. Compared to the previously published dataset by Kochtitzky *et al.*[13], the focus of this study is on fewer glaciers and with a higher temporal resolution, making the dataset more suitable for investigating the processes of terminus mass loss.

We also believe that the processing chain developed is a useful tool for quantifying frontal ablation for any glacier, as it is computationally inexpensive and can be easily modified.

Code availability

We provide the latest set of scripts (Version 9) that make up the processing chain used to produce the final frontal ablation product as well as example data for Helheim Glacier in the following Zenodo repository https://doi.org/10.5281/zenodo.8414729[41]. Given these scripts, a user can replicate the frontal ablation estimates, as well as calculate F at different time resolutions, swap in new input data, reproduce time series of uncertainties, and so forth.

Received: 1 August 2024; Accepted: 3 April 2025;
Published online: 10 April 2025

References

1. Enderlin, E. M. *et al*. An improved mass budget for the Greenland ice sheet. *Geophys Res Lett* **41**, 866–872 (2014).
2. Mouginot, J. *et al*. Forty-six years of Greenland Ice Sheet mass balance from 1972 to 2018. *Proceedings of the National Academy of Sciences* **116**, 9239 LP–9244 (2019).
3. Shepherd, A. *et al*. Mass balance of the Greenland Ice Sheet from 1992 to 2018. *Nature* **579**, 233–239 (2020).
4. Greene, C. A., Gardner, A. S., Wood, M. & Cuzzone, J. K. Ubiquitous acceleration in Greenland Ice Sheet calving from 1985 to 2022. *Nature* **625**, 523–528 (2024).
5. Cogley, J. G. *et al*. Glossary of glacier mass balance and related terms, IHP-VII technical documents in hydrology No. 86, IACS Contribution No. 2. International Hydrological Program. *UNESCO, Paris. doi* **10**, 1938–4246 (2011).
6. Cowton, T. R., Sole, A. J., Nienow, P. W., Slater, D. A. & Christoffersen, P. Linear response of east Greenland's tidewater glaciers to ocean/atmosphere warming. *Proceedings of the National Academy of Sciences* **115**, 7907–7912 (2018).
7. King, M. D. *et al*. Dynamic ice loss from the Greenland Ice Sheet driven by sustained glacier retreat. *Commun Earth Environ* **1**, 1 (2020).
8. Rignot, E. & Kanagaratnam, P. Changes in the velocity structure of the Greenland Ice Sheet. *Science (1979)* **311**, 986–990 (2006).
9. Osmanoğlu, B., Braun, M., Hock, R. & Navarro, F. J. Surface velocity and ice discharge of the ice cap on King George Island, Antarctica. *Ann Glaciol* **54**, 111–119 (2013).
10. McNabb, R. W., Hock, R. & Huss, M. Variations in Alaska tidewater glacier frontal ablation, 1985–2013. *J Geophys Res Earth Surf* **120**, 120–136 (2015).
11. Wagner, T. J. W. *et al*. Large spatial variations in the flux balance along the front of a Greenland tidewater glacier. *Cryosphere* **13**, 911–925 (2019).
12. Fried, M. J. *et al*. Reconciling Drivers of Seasonal Terminus Advance and Retreat at 13 Central West Greenland Tidewater Glaciers. *J Geophys Res Earth Surf* **123**, 1590–1607 (2018).
13. Kochtitzky, W. *et al*. Closing Greenland's Mass Balance: Frontal Ablation of Every Greenlandic Glacier From 2000 to 2020. *Geophys Res Lett* **50**, e2023GL104095 (2023).
14. Kochtitzky, W. *et al*. The unquantified mass loss of Northern Hemisphere marine-terminating glaciers from 2000–2020. *Nat Commun* **13**, 5835 (2022).
15. Bunce, C., Nienow, P., Sole, A., Cowton, T. & Davison, B. Influence of glacier runoff and near-terminus subglacial hydrology on frontal ablation at a large Greenlandic tidewater glacier. *Journal of Glaciology* **67**, 343–352 (2021).
16. Wychen, W. *et al*. RADARSAT-2 Derived Glacier Velocities and Dynamic Discharge Estimates for the Canadian High Arctic: 2015–2020. *Canadian Journal of Remote Sensing* **46**, 695–714 (2020).
17. Köhler, A. *et al*. A 15 year record of frontal glacier ablation rates estimated from seismic data. *Geophys Res Lett* **43**, 12,112–155,164 (2016).
18. Mankoff, K. D. *et al*. Greenland Ice Sheet solid ice discharge from 1986 through March 2020. *Earth Syst. Sci. Data* **12**, 1367–1383 (2020).
19. Colgan, W. *et al*. Glacier crevasses: Observations, models, and mass balance implications. *Reviews of Geophysics* **54**, 119–161 (2016).
20. Morlighem, M. *et al*. & others. BedMachine v3: Complete bed topography and ocean bathymetry mapping of Greenland from multibeam echo sounding combined with mass conservation. *Geophys Res Lett* **44** (2017).
21. Wood, M. *et al*. Ocean forcing drives glacier retreat in Greenland. *Sci Adv* **7**, eaba7282 (2021).
22. Morlighem, M. *et al*. IceBridge BedMachine Greenland. (IDBMG4, Version 5). [surface, bed, error]. *NASA National Snow and Ice Data Center Distributed Active Archive Center*. Boulder, Colorado USA. https://doi.org/10.5067/GMEVBWFLWA7X (2022)
23. Goliber, S. & Black, T. TermPicks: A century of Greenland glacier terminus data for use in machine learning applications (Version 1). *Zenodo* https://zenodo.org/records/5117931 (2021).
24. Goliber, S. *et al*. TermPicks: a century of Greenland glacier terminus data for use in scientific and machine learning applications. *Cryosphere* **16**, 3215–3233 (2022).
25. Porter, C. et al. ArcticDEM - Strips. Version 4.1, *Harvard Dataverse, V1*, [15/10/2024], https://doi.org/10.7910/DVN/C98DVS (2022).
26. Korsgaard, N. J. *et al*. Digital Elevation Model and orthophotographs of Greenland based on aerial photographs from 1978-1987 (G150 AERODEM) (NCEI Accession 0145405). *NOAA National Centers for Environmental Information*, https://doi.org/10.7289/v56q1v72 [10/08/2022] (2016).
27. Fan, Y., Ke, C.-Q. & Shen, X. A new Greenland digital elevation model derived from ICESat-2 during 2018–2019. *Earth Syst. Sci. Data* **14**, 781–794 (2022).
28. Khan, S. A. Greenland Ice Sheet Surface Elevation Change. *GEUS Dataverse v2*, https://doi.org/10.22008/FK2/GQJJEA (2023).
29. Mankoff, K., Solgaard, A., Larsen, S., PROMICE & program, I. under the E. U. H. 2020 research and innovation. Greenland Ice Sheet solid ice discharge from 1986 through last month: Discharge. *GEUS Dataverse, v100*, https://doi.org/10.22008/promice/data/ice_discharge/d/v02 (2020).
30. Gardner, A. S. *et al*. Increased West Antarctic and unchanged East Antarctic ice discharge over the last 7 years. *Cryosphere* **12**, 521–547 (2018).
31. Gardner, A. S., Fahnestock, M. A. & Scambos, T. A. ITS_LIVE Regional Glacier and Ice Sheet Surface Velocities, *Data archived at National Snow and Ice Data Center*. https://doi.org/10.5067/6II6VW8LLWJ7, [20/10.2024] (2019).
32. Greene, C. A., Gwyther, D. E. & Blankenship, D. D. Antarctic mapping tools for MATLAB. *Comput Geosci* **104**, 151–157 (2017).
33. Meier, M. *et al*. Mechanical and hydrologic basis for the rapid motion of a large tidewater glacier: 1. Observations. *J Geophys Res Solid Earth* **99**, 15219–15229 (1994).
34. Enderlin, E. M. *et al*. An Empirical Approach for Estimating Stress-Coupling Lengths for Marine-Terminating Glaciers. *Frontiers in Earth Science* **4**, https://www.frontiersin.org/articles/10.3389/feart.2016.00104 (2016)
35. Howat, I. M., Joughin, I., Fahnestock, M., Smith, B. E. & Scambos, T. A. Synchronous retreat and acceleration of southeast Greenland outlet glaciers 2000–06: Ice dynamics and coupling to climate. *Journal of Glaciology* **54**, 646–660 (2008).
36. Howat, I. M., Joughin, I., Tulaczyk, S. & Gogineni, S. Rapid retreat and acceleration of Helheim Glacier, east Greenland. *Geophys Res Lett* **32** (2005).
37. Fahrner, D., Lea, J. M., Brough, S., Mair, D. W. F. & Abermann, J. Linear response of the Greenland ice sheet's tidewater glacier terminus positions to climate. *Journal of Glaciology* **67**, 193–203 (2021).
38. Brough, S., Carr, J. R., Ross, N. & Lea, J. M. Exceptional retreat of Kangerlussuaq Glacier, east Greenland, between 2016 and 2018. *Front Earth Sci (Lausanne)* **7** (2019).
39. Fahrner, D. *et al*. Frontal ablation estimates for 49 tidewater glaciers in Greenland. *Zenodo* https://doi.org/10.5281/zenodo.10076252 (2025).
40. Joughin, I. *et al*. Continued evolution of Jakobshavn Isbrae following its rapid speedup. *J Geophys Res Earth Surf* **113** (2008).
41. Fahrner, D. *et al*. Tidewater Glacier Frontal Ablation Tool - TG_FACT. *Zenodo* https://doi.org/10.5281/zenodo.8414729 (2025).

Acknowledgements

We thank two anonymous reviewers and the editor for their helpful comments. DF acknowledges support from the Novo Nordisk Foundation under the Challenge Programme 2023 grant number NNF23OC00807040. TJWW acknowledges support from the National Science Foundation Office of Polar Programs (grant nos. 2148544 and 2338057). DAS acknowledges support from NERC Independent Research Fellowship NE/T011920/1. DEMs provided by the Polar Geospatial Center under NSF-OPP awards 1043681, 1559691, 1542736, 1810976, and 2129685.

Author contributions

D.F. and all co-authors conceived the study. D.F. created the processing chain, pre-processed the data, conducted all data analysis, figure production, and led the manuscript writing. All co-authors provided conceptual and technical advice and contributed to manuscript writing.

Competing interests

The authors declare no competing interests.

Additional information

Supplementary information The online version contains supplementary material available at https://doi.org/10.1038/s41597-025-04948-3.

Correspondence and requests for materials should be addressed to D.F.

Reprints and permissions information is available at www.nature.com/reprints.

Publisher's note Springer Nature remains neutral with regard to jurisdictional claims in published maps and institutional affiliations.